# Lateral Transport Controls the Tidally Averaged Gravitationally Driven Estuarine Circulation: Tidal Mixing Effects

Tobias Kukulka<sup>a</sup> and Robert J. Chant<sup>b</sup>

<sup>a</sup> University of Delaware, Newark, Delaware <sup>b</sup> Rutgers University, New Brunswick, New Jersey

(Manuscript received 1 November 2023, in final form 1 April 2024, accepted 19 April 2024)

ABSTRACT: In classic models of the tidally averaged gravitationally driven estuarine circulation, denser salty oceanic water moves up the estuary near the bottom, while less dense riverine water flows toward the ocean near the surface. Traditionally, it is assumed that the associated pressure gradient forces and salt advection are balanced by vertical mixing. This study, however, demonstrates that lateral (across the estuary width) transport processes are essential for maintaining the estuarine circulation. This is because for realistic estuarine bathymetry, the depth-integrated salt transport up the estuary is enhanced in the deeper estuary channel. A closed salt budget then requires the lateral transport of this excess salt in the deeper channel toward the estuarine flanks. To understand how such lateral transport affects the estuarine salt and momentum balances, we devise an idealized model with explicit lateral transport focusing on tidally averaged lateral mixing effects. Solutions for the along-estuary velocity and salinity are nondimensionalized to depend only on one single nondimensional parameter, referred to as the Fischer number, which describes the relative importance of lateral to vertical tidal mixing. For relatively strong lateral tidal mixing (greater Fischer number), salinity and velocity variations are predominantly vertical. For relatively weak lateral tidal mixing (smaller Fischer number), salinity and velocity variations are predominantly lateral. Overall, lateral transport greatly affects the estuarine circulation and controls the estuarine salinity intrusion length, which is demonstrated to scale inversely with the Fischer number.

KEYWORDS: Estuaries; Channel flows; Coastal flows; Density currents; Dispersion; Secondary circulation

#### 1. Introduction

The estuarine circulation, also called the estuarine exchange flow, controls unique estuarine habitat and ecosystem dynamics, drives land-ocean interactions, and transports sediments, nutrients, and organisms, as well as pollutants. The cornerstone of the basic conceptual estuarine circulation theory is the classic analysis of the tidally averaged circulation, revealing the strength of the exchange flow and structure of the salinity distribution (Hansen and Rattray 1965; MacCready and Geyer 2010). The theory assumes that the along-channel pressure gradient is balanced by a vertical turbulence stress divergence in the presence of tidal mixing. The pressure gradient arises from an oceanward down-sloping sea surface and an along-channel salinity (density) gradient. This force balance yields a circulation whereby saline ocean water moves landward in the lower layer with a fresher seaward flow in the upper layer. The along-estuary salt straining associated with this circulation is assumed to be balanced entirely by vertical turbulent mixing. Thus, the exchange flow acting on the salinity stratification drives a landward salt flux that, in the absence of a net salt flux due to tidal motion, is balanced by a seaward salt flux due to the river discharge. While this insightful conceptual framework is known to be oversimplified for a host of reasons (e.g., Jay and Musiak 1994; Monismith et al. 2002; Lerczak and Geyer 2004; Ralston et al. 2008; Burchard et al. 2011; Aristizábal and Chant 2013; Geyer and MacCready 2014), here, we demonstrate that lateral, i.e.,

Corresponding author: Tobias Kukulka, kukulka@udel.edu

directed horizontally and across the estuary, transport processes are essential in maintaining the tidally averaged gravitationally driven estuarine circulation focusing on lateral tidal mixing effects.

To understand the need for lateral transport processes intuitively, it is instructive to consider the simplified classic salt budget in which salt advection due to the exchange flow and along-channel salinity gradients is balanced by the vertical divergence of turbulent salt fluxes. Without salt fluxes through the bottom and surface of the estuary, vertical turbulent mixing of salt only redistributes salt vertically. However, the depthintegrated salt advection is generally nonzero because the along-estuary velocity varies laterally so that depth-averaged along-estuary velocities are up-estuary near the deeper channel and toward the ocean near the flanks (e.g., Fischer 1972; Wong 1994). Consequently, a closed salt budget requires the lateral transport of excess salt close to the deeper channel to regions with salt deficits near the flanks (more formal arguments are presented in the next section).

In estuaries with a deeper channel and shallow flanks, observations show that both the exchange flows and the salinity distribution develop strong lateral gradients (Wong 1994; Valle-Levinson and Atkinson 1999; Valle-Levinson et al. 2000) and this lateral variability in momentum and density drives lateral flows that result in lateral mixing (Nunes and Simpson 1985; Huzzey and Brubaker 1988; Lacy et al. 2003; Lerczak and Geyer 2004). It is important to distinguish between two different time scales of lateral advection processes: 1) lateral advection driven by tidally averaged lateral salinity gradients (e.g., Smith 1976), which is not the focus of this

paper, and 2) tidally averaged effects of tidally resolved lateral advection, which is related to lateral tidal mixing processes.

As a first step, this study focuses on lateral tidal mixing fluxes that are linked to processes due to tidally resolved lateral flows (Lerczak and Geyer 2004; Scully et al. 2009; Burchard et al. 2011; Li et al. 2014). For example, tidally varying axial convergence flows move saltier to fresher water (or fresher to saltier water depending on the tidal phase and vertical location), contributing to the increase of lateral mixing (e.g., Nunes and Simpson 1985). The detailed physics of the tidally averaged lateral mixing are complicated and expected to be associated with complex bathymetry and shoreline irregularities (Fischer 1976) in conjunction with tidally resolved processes, for example, related to strong lateral shears (Taylor 1953; Geyer et al. 2008) and secondary cellular flows (Majda and Kramer 1999; Thoman et al. 2021). Fischer (1972) found that lateral mixing critically influences the along-estuary dispersion of tracers, and Fischer (1976) suggested that lateral mixing scales with tidal velocity and depth or estuary width. In particular, Fischer (1972) emphasized that the relative importance of vertical to lateral shear dispersion due to the along-estuary velocity is controlled by a nondimensional parameter, here referred to as the Fischer number  $\gamma$ , that can be interpreted as the ratio of a vertical mixing time scale to lateral mixing time scale. In this paper, we introduce a related nondimensional mixing number  $\gamma$  that describes the relative importance of lateral to vertical tidal mixing to demonstrate that  $\gamma$  determines the structure of the exchange flow, the salinity distribution, and, ultimately, the landward flux of salt for estuarine systems in which lateral tidal mixing fluxes are important relative to tidally averaged advection.

The goal of this paper is to devise a simple conceptual model that 1) extends the classic estuarine circulation framework through the inclusion of lateral transport focusing on lateral tidal mixing fluxes, 2) closes both the momentum and salt mass budgets based on coupled conservation equations, and 3) is intuitive to understand and analytically tractable. In the next section (section 2), we introduce nondimensional balance equations with lateral fluxes and then present a theory for tidal-mixing-flux-dominated regimes (section 3) before exploring an illustrative test case (section 4). Section 5 discusses constraints and limitations of key model parameters. The conclusions (section 6) highlight that both the spatial structure and magnitude of the tidally averaged estuarine circulation and salinity distribution critically depend on estuarine lateral transport processes affecting the estuarine salinity intrusion length.

## 2. Theory: Estuarine gravitational circulation with lateral transport

As a first step to shed light on lateral transport processes, we will start from the classic theoretical framework of the tidally averaged estuarine circulation (see review by MacCready and Geyer 2010). Therefore, we neglect here explicit tidally resolved effects, for example, related to tidally variable mixing and tidally driven residual circulations (Jay and Musiak

1994; see also the review by Geyer and MacCready 2014). For simplicity, we also omit the Coriolis force which may play an important role in driving lateral circulations (Valle-Levinson 2008).

Specifically, we consider the transport in an idealized estuary with a constant cross section of the maximum width B and the laterally varying depth h(y) both of which are assumed constant along the estuary. The channel shall be mirror symmetric around its maximum depth  $h_0$  in the channel center. We define the tidally averaged along-channel velocity  $\mathcal{U}$  and salinity S and assume that  $\mathcal{U}$  and S are in steady state. Next, we decompose variables into cross-sectionally averaged ones and their corresponding deviations, denoted by uppercase and lowercase, respectively, so that U = U(x) + u(x, y, z) and S = S(x) + s(x, y, z). Here, x is the along-estuary coordinate with x = 0 at the mouth so that x < 0 decreases up-estuary, y is the lateral (horizontal and across the estuary) coordinate with y = 0 in the channel center, and z is the vertical coordinate with z = 0 at the air-water interface and z increases upward. The depth and cross-sectional average of the lateral vand vertical w velocities are, respectively, zero. Because U is assumed to be constant, we have dU/dx = 0. As a first step, we consider a two-dimensional problem so that we neglect  $u_r$ and  $s_x$  (consistent with Burchard et al. 2011). We define an overline as the horizontal average  $\overline{(\cdot)} = B^{-1} \int_{-B/2}^{B/2} (\cdot) dy$  and angle brackets as y-dependent vertical integration over the water column  $\langle (\cdot) \rangle = \int_{-h}^{0} (\cdot) dz$ , so that the cross-sectional average is  $(\overline{h})^{-1}\overline{\langle \mathcal{U} \rangle} = U$  and  $(\overline{h})^{-1}\overline{\langle \mathcal{S} \rangle} = S$ .

## a. Momentum and salt mass balances with lateral transport

Similar to Smith (1976), we first consider two lateral transport processes due to 1) tidally averaged advection due to tidally averaged lateral salinity gradients, which is neglected later, and 2) lateral tidal mixing, which mix properties from high to low concentrations and is the focus of this study. We parameterize such lateral tidal mixing fluxes via a downgradient assumption and introduce lateral mixing coefficients for momentum  $K_{MY}$  and salt  $K_{SY}$ . The governing Reynolds-averaged equations for u, v, and s are obtained by adding lateral transport processes to the traditional one-dimensional equations that govern only vertical variability (Smith 1976), while the conservation equation for S is taken unchanged from the traditional framework (see, e.g., Hansen and Rattray 1965; MacCready and Geyer 2010)

$$0 = -g\eta_x + g\beta S_x z + K_{MZ} u_{zz} + K_{MY} u_{yy} - (uw)_z - (uv)_y,$$
(1)

$$0 = -g\eta_{y} + g\beta \int_{z}^{0} s_{y}(\tilde{z})d\tilde{z} + K_{MZ}v_{zz} + K_{MY}v_{yy} - (vw)_{z} - (vv)_{y},$$

$$(2)$$

$$uS_{x} = K_{SZ}s_{zz} + K_{SY}s_{yy} - (sw)_{z} - (sv)_{y},$$
(3)

$$US + (\overline{h})^{-1} \overline{\langle us \rangle} = K_X S_x, \tag{4}$$

where g is the acceleration of gravity,  $\eta$  is the air–water interfacial displacement height,  $\beta=7.7\times10^{-4}$  is the haline contraction coefficient,  $K_X$  is an along-channel eddy diffusivity due to tidal mixing, and  $K_{MZ}$  and  $K_{SZ}$  symbolize the vertical eddy viscosity and diffusivity, respectively. Here, we assume that mixing coefficients are constant. Subscripts of lowercase variables indicate partial derivatives with respect to that variable, e.g.,  $u_z=\partial u/\partial z$ . The vertical velocity w is determined from the continuity equation  $0=v_y+w_z$ . The boundary conditions are

$$u_z = v_z = 0$$
  $w = 0$  at  $z = 0$ ,  
 $u = v = w = 0$  at  $z = -h(y)$ , (5)

$$s_z = 0 \quad \text{at} \quad z = 0,$$
 
$$K_{SZ}s_z + K_{SY}s_yh_y = 0 \quad \text{at} \quad z = -h(y), \quad \text{and} \qquad (6)$$

$$S = S_0 \quad \text{at} \quad x = 0, \tag{7}$$

where  $S_0$  is the salinity at the estuarine mouth. The surface boundary condition for u and v is a zero stress condition, while w satisfies a zero volume flux condition. At the bottom, u, v, and w satisfy the no-slip conditions. No flux conditions are imposed for s at the vertical boundaries. Note that the bottom boundary conditions can alternatively be formulated at  $y = \pm (1/2)b(z)$ , where b(z) is the z-dependent channel width.

#### b. Nondimensional equations

To understand the behavior of solutions, we will first consider key scales and nondimensional parameters. For the following analysis, we focus on the case for which the magnitude of U is sufficiently small compared to that of u, so that the river flow shall not be considered in the momentum balance (1), which is a common assumption for process-based studies (e.g., Burchard et al. 2011). We introduce the following nondimensional variables:

$$u' = u_S^{-1}u, \quad v' = v_S^{-1}v, \quad w' = \delta^{-1}v_S^{-1}w,$$
  
 $s' = s_S^{-1}s, \quad y' = yB^{-1}, \quad z' = zh_0^{-1},$  (8)

where the along-estuary and the lateral scaling velocity  $u_S$  and  $v_S$  and the salinity scaling  $s_S$  are, respectively, given by

$$u_{S} = g\beta S_{x}h_{0}^{3}K_{MZ}^{-1}, \quad v_{S} = u_{S}s_{S}(S_{x}B)^{-1},$$
  

$$s_{S} = g\beta S_{x}h_{0}^{3}K_{MZ}^{-1}K_{SZ}^{-1}h_{0}^{2}S_{x} = u_{S}K_{SZ}^{-1}h_{0}^{2}S_{x}.$$
(9)

Note that  $u_S$  is the traditional velocity scale for the residual circulation (Hansen and Rattray 1965; MacCready and Geyer 2010). The nondimensional along-estuary and across-estuary slopes and depth scale, respectively, are

$$\eta_x' = \eta_x (\beta h_0 S_x)^{-1}, \quad \eta_y' = \eta_y B (\beta h_0 S_S)^{-1}, \quad h' = h h_0^{-1}.$$
(10)

Note that this scaling assumes strong lateral variability because the depth and lateral changes of depth both scale as  $h_0$ .

With this scaling, the following nondimensional parameters

$$\delta = \frac{h_0}{B}, \quad \kappa_M = \frac{K_{MY}}{K_{MZ}}, \quad \kappa_S = \frac{K_{SY}}{K_{SZ}},$$

$$\mu_M = \frac{Bv_S}{K_{MZ}}, \quad \mu_S = \frac{Bv_S}{K_{SZ}},$$
(11)

where  $\delta$  represents the depth-to-width aspect ratio and is the only parameter that explicitly includes width B. After dropping all primes, the nondimensional u, v, and s equations are, respectively,

$$\eta_x - z = u_{zz} + \kappa_M \delta^2 u_{yy} - \mu_M \delta^2 (uw)_z - \mu_M \delta^2 (uv)_y,$$
 (12)

$$\eta_{y} - \int_{z}^{0} s_{y}(\tilde{z}) d\tilde{z} = v_{zz} + \kappa_{M} \delta^{2} v_{yy} - \mu_{M} \delta^{2} (vw)_{z}$$
$$- \mu_{M} \delta^{2} (vv)_{y}, \tag{13}$$

$$u = s_{zz} + \kappa_S \delta^2 s_{yy} - \mu_S \delta^2 (sw)_z - \mu_S \delta^2 (sv)_y.$$
 (14)

These equations demonstrate that  $\delta^2 \kappa_M$  represents the relative importance of lateral to vertical tidal mixing fluxes,  $\delta^2 \mu_M$  represents the relative importance of advective to vertical turbulent fluxes, and  $\kappa_M(\mu_M)^{-1}$  represents the relative importance of lateral tidal mixing to lateral advective fluxes (similar applies for corresponding nondimensional ratios related to  $\kappa_S$  and  $\mu_S$ ). The boundary conditions are

$$u_z = v_z = 0$$
  $w = 0$  at  $z = 0$ ,  
 $u = v = w = 0$  at  $z = -h(y)$ , (15)

$$s_z = 0$$
 at  $z = 0$ ,  $s_z + \delta^2 \kappa_S s_y h_y = 0$  at  $z = -h(y)$ . (16)

These governing equations highlight that for  $K_S = K_M$ , the problem is determined by two key nondimensional numbers, namely,  $\delta^2 \kappa_M$  and  $\delta^2 \mu_M$ . It is insightful to vertically integrate the salt balance over the water column to obtain after applying the boundary conditions

$$\langle u \rangle = \kappa_S \delta^2 \langle s_v \rangle_v - \mu_S \delta^2 \langle (sv)_v \rangle,$$
 (17)

where the last equation demonstrates the general need for lateral transport terms to close the salt budget. In the remaining part of this paper, we will focus on lateral transport that is dominated by tidal mixing fluxes.

### 3. Application to tidal-mixing-dominated regimes

We first consider the scaling for a tidal-mixing-flux-dominated regime and then discuss approximate solutions, before revealing implications for the along-estuary salt balance.

a. Scaling lateral advection relative to tidal mixing fluxes

The nondimensional equations suggest that lateral tidal mixing fluxes are dominant over advection for  $\kappa_{MS}(\mu_{MS})^{-1} \gg 1$ ,

so that advection terms are small relative to lateral tidal mixing flux terms. This condition, however, is generally too restrictive because lateral tidal mixing also reduces lateral salinity gradients and, therefore, lateral advection. In addition, advection is inefficient for shallow water with  $\delta \ll 1$ . This can be understood by considering that for  $\delta \ll 1$ , (12) and (13) suggest that the pressure gradient terms on the left-hand side are balanced by vertical turbulent fluxes, and lateral transport and advection are negligible to leading order consistent with the classic theory (Hansen and Rattray 1965; Smith 1976; Nunes and Simpson 1985). For the salt balance [(14)], however, salt advection cannot be balanced by vertical turbulent mixing alone as (17) establishes. Therefore, to leading order, (14) can only be satisfied for  $s_{zz} = 0$ , so that  $s_z = 0$  because of the boundary conditions [(16)]. This however implies with  $\langle v \rangle = 0$ that the advective term in (17) is inefficient in moving salt laterally, so that advective terms are overall negligible for shallow-water systems with  $\delta \ll 1$ . These arguments will be assessed and explored in detail in a follow-up study. Here, we focus for the remaining paper on conditions for which  $\kappa_{M,S}(\mu_{M,S})^{-1} \gg 1$  or  $\delta \ll 1$  so that the resolved advection is negligible relative to lateral tidal mixing fluxes.

After defining the two key nondimensional parameters  $\gamma_M = \delta^2 \kappa_M$  and  $\gamma_S = \delta^2 \kappa_S$ , the governing nondimensional u and s equations become, respectively,

$$\eta_x - z = u_{zz} + \gamma_M u_{yy}, \tag{18}$$

$$u = s_{zz} + \gamma_S s_{vv}, \tag{19}$$

with the same boundary conditions for u and s given by (15) and (16). Equation (18) illustrates that u depends only on the cross-sectional geometry h(y) and the independent variables y and z, as well as parametrically on  $\gamma_M$ , which controls the relative importance of lateral to vertical transport of u. Note that  $B^2K_{MY}^{-1}$  and  $h_0^2K_{MZ}^{-1}$  represent lateral and vertical mixing time scales, respectively, so that  $\gamma_M$  is related to the ratio of vertical to lateral mixing time scales. Equation (19) reveals that solutions for s depend on both u and parametrically on  $\gamma_{S}$ , describing the relative importance of lateral to vertical tidal mixing salt fluxes.

This simple scaling analysis highlights that  $\gamma_M$  and  $\gamma_S$  are key model parameters that determine the solutions of u and s. In this study, we refer to  $\gamma_M$  or  $\gamma_S$  as the Fischer number (for momentum and salt) because  $\gamma_M$  was originally introduced by Fischer (1972), suggesting that this parameter determines the effects on longitudinal dispersion due to the lateral relative to vertical shear of the along-channel gravitational circulations.

### b. Approximate analytic solutions

To understand how lateral transport due to tidal mixing and the Fischer parameter control u and s, we will first explore the small and large limits of  $\gamma_M$  and  $\gamma_S$ .

## 1) WEAK LATERAL TIDAL MIXING $(\gamma_M, \gamma_S \ll 1)$

In the weak lateral mixing case  $\gamma_M$ ,  $\gamma_S \ll 1$ , friction is dominated by vertical stresses and one may neglect lateral stresses

to leading order in the momentum equation (so that narrow lateral frictional boundary layers are neglected too), which is consistent with the classic estuarine circulation theory and, by vertically integrating (18) twice and applying the boundary conditions, the solution is

$$u(y, z) = \frac{1}{6} (3\eta_x \{z^2 - [h(|y|)]^2\} - \{z^3 + [h(|y|)]^3\}).$$
 (20)

Note that generally this solution is characterized by significant lateral variability if the depth varies sufficiently laterally. This solution is consistent with the shallow-water asymptotic expansion solution from Smith (1976) and is a more general version than the one for bilinear channel cross section (Fischer 1972; Wong 1994). Remember that  $\eta_x$  is determined here so that the cross-sectionally averaged u vanishes (in a more general approach, the cross-sectionally integrated u should be equal to the river discharge). For example, for a bilinear depth profile h(y), one finds  $\eta_x = -3/10$ . For a flat bottom, i.e., h = constant, the solution is consistent with the classic solution (Hansen and Rattray 1965) and  $\eta_x = -3/8$ .

The situation is different for the salt balance because of the no salt flux through the bottom and surface boundary conditions: A relatively strong vertical transport nearly homogenizes s vertically, so that  $s_z \approx 0$  and  $h^{-1}\langle s \rangle \approx s$ . An approximate solution may then be readily found for s through a double lateral integration of (17) (neglecting advective terms)

$$s(y) = c_{s0} + \gamma_S^{-1} \int_0^{|y|} \frac{1}{h(\hat{y})} \int_0^{\hat{y}} \langle u \rangle d\tilde{y} d\hat{y}, \tag{21}$$

where  $c_{s0}$  is a constant of integration to satisfy  $\overline{\langle s \rangle} = 0$ . This solution also yields the important scaling result  $s \propto \gamma_s^{-1}$ . Physically, this result states that for relatively small  $\gamma_s$ , e.g., for relatively small  $K_{SY}$  and less efficient lateral transport, salinity differences between the saltier channel center and fresher regions closer to shore are relatively large as expected. Combining the last result with (20), we find that the salt flux in (4) due to the estuarine residual circulation scales as

$$\overline{\langle us \rangle} \propto \gamma_S^{-1}$$
. (22)

The last scaling illustrates that the cross-sectionally averaged along-estuary salt flux increases with decreasing  $\gamma_S$  (or  $K_{SY}$ ). This result is remarkable as lateral transport, although assumed to be relatively small, still controls the along-estuary salt flux. This is because the weaker lateral salt transport enhances the lateral s variability, thereby increasing the along-estuary salt flux as u remains unchanged. Furthermore, variability in the exchange flow is predominantly lateral unlike the classic picture because s is approximately constant with depth.

## 2) Strong lateral tidal mixing $(\gamma_M, \gamma_S \gg 1)$

Our study indicates that lateral tidal mixing fluxes are likely a substantial process for many estuarine systems, and it is therefore insightful to consider theoretically the system's behavior and associated approximate solutions for strong lateral tidal mixing fluxes. Contrary to the previous case, for sufficiently strong lateral transport, i.e.,  $\gamma_M$ ,  $\gamma_S \gg 1$ , momentum fluxes are expected to be dominated by lateral stresses and one may neglect vertical stresses to leading order in the momentum equation (so that narrow vertical frictional boundary layers are neglected too) and the solution to (18) without turbulent vertical fluxes is approximated by

$$u(y, z) = \frac{1}{2} \gamma_M^{-1} (\eta_x - z) \left\{ y^2 - \left[ \frac{b(z)}{2} \right]^2 \right\}, \tag{23}$$

where b(z) is the *B*-normalized *z*-dependent estuary width. Thus, u is proportional to  $\gamma_M^{-1}$ . Note that this solution differs fundamentally from the traditional estuarine circulation theory as driving along-channel pressure gradient forces are entirely balanced by lateral friction.

Following analogous arguments as for the weak lateral mixing case, a relatively strong lateral transport is expected to homogenize s laterally, so that  $s_y \approx 0$  and  $\bar{s} \approx s$ . This time, we laterally integrate (19) to obtain after incorporation of the boundary conditions [(16)]

$$\int_{-b(z)/2}^{b(z)/2} u dy = (bs_z)_z.$$
 (24)

The last equation is readily integrated twice with respect to z

$$s(z) = c_{s\infty} + \int_{-1}^{z} \frac{1}{b(\hat{z})} \int_{\hat{z}}^{0} \int_{-b(\bar{z})/2}^{b(\bar{z})/2} u dy d\tilde{z} d\hat{z},$$
 (25)

where  $c_{s\infty}$  is a constant of integration to satisfy  $\overline{\langle s \rangle} = 0$ . This solution yields the important scaling result  $s \propto \gamma_M^{-1}$  because of  $u \propto \gamma_M^{-1}$  and with (23)

$$\overline{\langle us \rangle} \propto \gamma_M^{-2}$$
. (26)

Therefore, the salt flux is, with the quadratic dependence  $\gamma_M^{-2}$ , more strongly dependent on lateral mixing compared to the weak lateral mixing case. Furthermore, the estuarine exchange flow is suppressed by greater  $K_{MY}$ , similar to the suppressed flow for greater  $K_{MZ}$  in the classic estuarine circulation theory (recall the dimensional  $u \propto u_S$  and  $u_S \propto K_{MZ}^{-1}$ ). As in classic theory, the exchange flow is approximately vertical because s mainly depends on s. Note, however, that salt is laterally homogenized by a relatively strong lateral salt transport, as (25) assumes negligible lateral variability.

## c. Implications for the along-estuary cross-sectionally averaged salt balance

The along-channel salt balance (4) is nondimensionalized following previous approaches (MacCready and Geyer 2010), except that the exchange flow term now also depends on  $\gamma_M$  and  $\gamma_S$ 

$$S - \Gamma^3 L_E^3 S_x^3 = L_H S_x, (27)$$

where  $L_E = \{[(g\beta h_0^2)^2/U][h_0^6/(K_{MZ}^2K_{SZ})]\}^{1/3}$  and  $L_H = K_X/U$  are the along-estuarine length scales associated with the

exchange flow and along-estuarine tidal mixing, respectively, and the nondimensional exchange flow parameter is defined as

$$\Gamma^{3}(\gamma_{M}, \gamma_{S}) = -(\overline{h})^{-1} \overline{\langle us \rangle}. \tag{28}$$

Note that for classic estuarine circulation theories,  $\Gamma=0.024$  (MacCready and Geyer 2010). For the weak and strong lateral transport cases discussed above,  $\Gamma^3 \propto \gamma_S^{-1}$  and  $\Gamma^3 \propto \gamma_M^{-2}$ , respectively, and the salt intrusion length scales as  $L_E \gamma_S^{-1/3}$  and  $L_E \gamma_M^{-2/3}$ , respectively. The constant of proportionality can be readily obtained for a specific lateral depth profile from the approximate analytic or numeric solutions, as discussed below (section 4). Note that  $\gamma_S = \gamma_M$  for  $K_{MZ} = K_{SZ}$ ,  $K_{MY} = K_{SY}$  and that  $\gamma_S/\gamma_M$  is related to turbulent Schmidt numbers. Thus, this scaling predicts that a relatively strong lateral transport and relatively narrow estuaries result in a substantial decrease in the estuarine salt intrusion length.

Once  $\Gamma$  is determined from the solutions of u and s, an exact analytic solution for  $S_x$  can be derived for constant eddy mixing coefficients by differentiating (27) with respect to x and then integrating the resulting equation with respect to  $S_x$  (i.e., swapping the dependent and independent variables) to obtain

$$x = \frac{3}{2} \Gamma^3 L_E^3 (S_x^2 - S_{x0}^2) + L_H \ln \frac{S_x}{S_{x0}},$$
 (29)

where  $S_{x0}$  is the salinity gradient at x=0 obtained from (4) with the boundary condition  $S=S_0$ . Solution (29) is an implicit solution for  $S_x$  so that  $x(S_x)$ . Because of the inverse relation between  $\Gamma$  and  $\gamma_{M/S}$ , (29) suggests that the along-estuary tidal mixing term becomes dominant over the exchange flow term for a sufficiently strong lateral mixing. Focusing on the estuarine exchange flow by the gravitational circulation, we explore the Chatwin (1976) approximation and neglect the along-estuary tidal mixing so that  $L_H=0$  and

$$S_x = \left[ \frac{2}{3\Gamma^3 L_E^3} x + (\Gamma L_E)^{-2} S_0^{2/3} \right]^{1/2}.$$
 (30)

Note that  $S_x(0) = S_{x0}$  is consistent with (27). Defining next the estuary intrusion length  $x_L$  where  $S_x$  is zero, we find

$$x_L = -\frac{3}{2}\Gamma L_E S_0^{2/3},\tag{31}$$

which highlights the importance of lateral transport in setting the estuarine salt intrusion length.

## 4. Illustrative example: Wong's (1994) model revisited

To provide an illustrative example, we revisit the estuarine circulation model for a bilinear depth profile for which h(y) decreases linearly from h=1 at y=0 to h=0 at  $y=\pm 1/2$  (Fig. 1) (Fischer 1972; Wong 1994). We solve (18) and (19) using an iterative, conservative second-order finite-difference approach. We employ a nested iteration approach for the determination of the barotropic pressure gradient coefficient  $\eta_x$  to satisfy  $\overline{\langle u \rangle} = 0$ . Through trial and error, we found that a

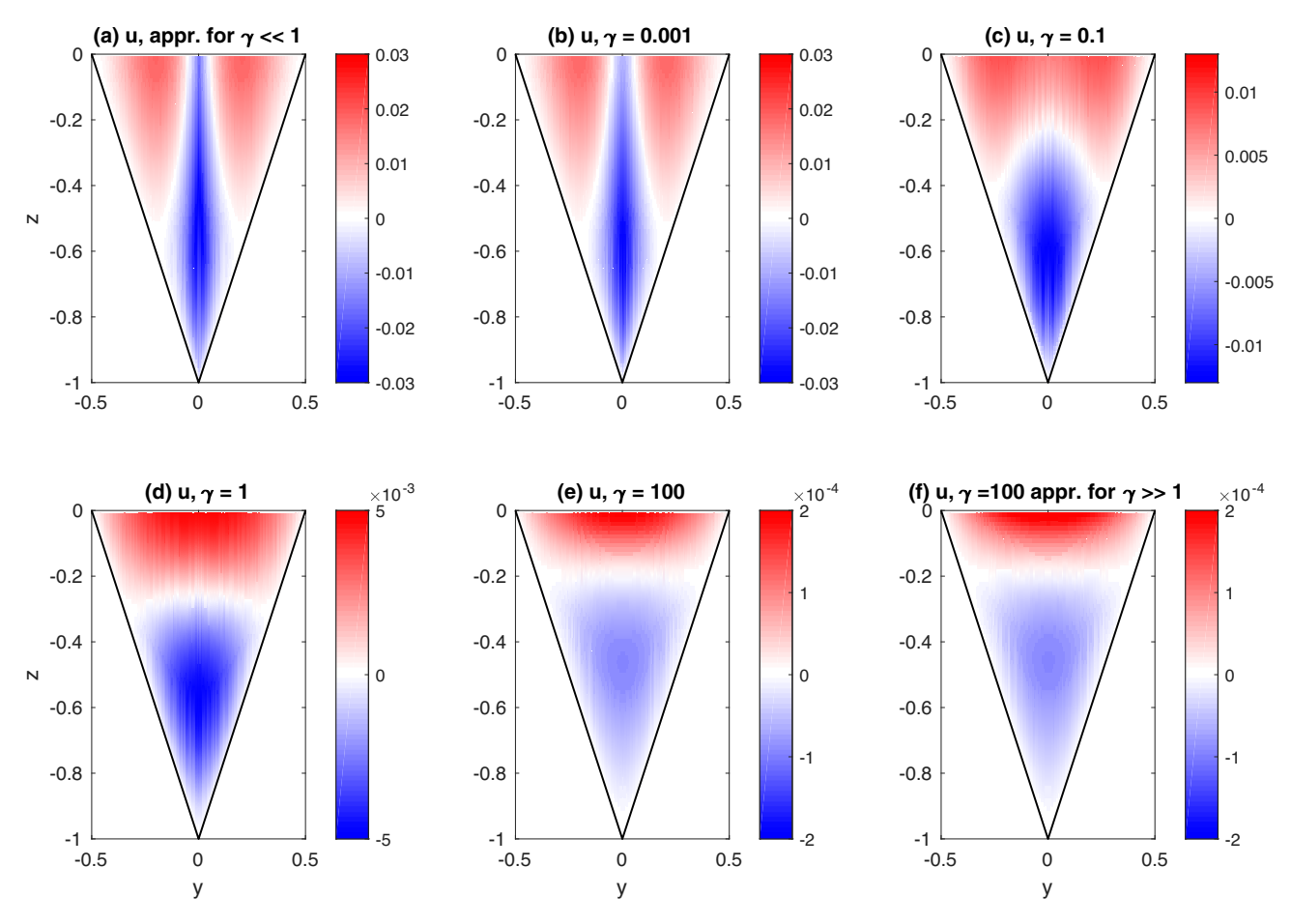


FIG. 1. Nondimensional solutions of u(y, z). (b)–(e) Numeric solutions for representative  $\gamma$  values and analytic approximation for (a)  $\gamma = 0$  ( $\gamma \ll 1$ ) and (f)  $\gamma = 100$  ( $\gamma \gg 1$ ).

maximum number of 151 lateral and 75 vertical grid points resolves sufficiently accurately u and s. For all computations, we set  $K_{SZ} = K_{MZ}$  and  $K_{SY} = K_{MY}$  so that we define for simplicity a single  $\gamma = \gamma_S = \gamma_M$ . Note that solutions for u and s only depend parametrically on  $\gamma$  so that solutions can be rescaled by  $u_S$  and  $s_S$  from (9) to any arbitrary choice of the other free model parameters B,  $h_0$ ,  $K_{MZ}$ , and  $S_x$ . We compute solutions of u and s for a wide range of  $\gamma$  from  $\gamma = 0.001$  to  $\gamma = 100$  to explore the full range of possible solutions from weak to strong lateral tidal mixing transport.

#### a. Numeric solutions of u and s

Figure 1 shows numeric solutions of nondimensional u for representative  $\gamma$  values (Figs. 1b–e) and the approximations for weak lateral transport with  $\gamma \ll 1$  [(20)] (Fig. 1a) and for strong lateral transport with  $\gamma \gg 1$  [(23)] (Fig. 1f). Note that the approximation for  $\gamma \ll 1$  is the same solution as presented in Wong (1994). The good agreement confirms the validity of the weak and strong lateral mixing approximation and their physical assumptions. For smaller  $\gamma$ , u is characterized by up-estuary velocities in the channel and flows toward the ocean closer to shore as expected (Wong 1994). As  $\gamma$  increases, the two-dimensional flow structure transitions from being predominantly lateral to including substantial vertical

variability. Only for greater  $\gamma$  does the flow resemble the one expected from classic theory with deeper flows up the estuary and more near-surface flows toward the ocean. However, the flow dynamics are entirely different from classic theory as vertical momentum fluxes are negligible over most parts of the channel for sufficiently large  $\gamma$ .

Figure 2 shows numeric solutions of nondimensional s for representative γ values (Figs. 2b-e). Fig. 2a presents the approximate solution of the normalized depth-integrated s based on (21) for weak lateral transport with  $\gamma \ll 1$  and a comparison to the result obtained from the full two-dimensional (2D) numeric solution. Figure 2f shows the other extreme comparing the approximate solution of the normalized laterally integrated s based on (25) for strong lateral transport with  $\gamma \gg 1$ to the full 2D numeric solution. These approximations agree well, both quantitatively and qualitatively, with the 2D numeric solutions, suggesting that the approximations capture well the leading-order dynamics. In particular, for small  $\gamma$ , the structure of s is characterized by substantial lateral variability with saltier water in the channel center. When lateral tidal mixing fluxes are weaker, such lateral salinity variability may drive lateral density currents to set up a negative feedback limiting lateral variability, which is explored in a follow-up study. Therefore, it is important to keep in mind that solutions

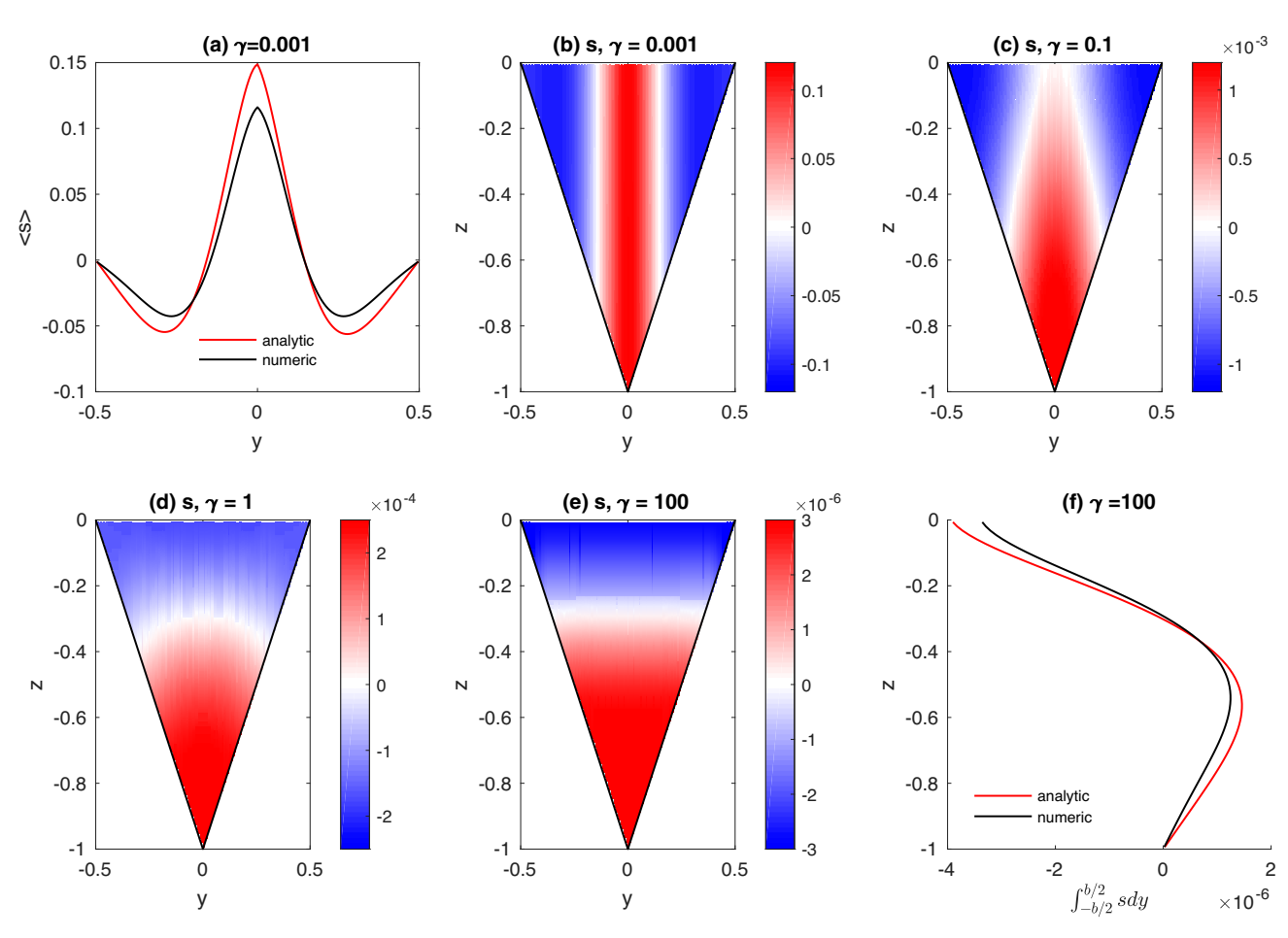


FIG. 2. Nondimensional salinity distributions. (b)–(e) Numeric 2D solution salinity s(y, z) and comparison of analytic and numeric solutions for (a) depth-averaged integrated s,  $\langle s \rangle$ , with  $\gamma = 0.001$  and (f) laterally integrated s with  $\gamma = 100$ .

for smaller  $\gamma$  without advection are only applicable for sufficiently shallow water so that  $\delta \ll 1$  or  $\gamma \gg \delta^2 \mu_{M,S}$ . Similar to u, increasing  $\gamma$  shifts the salinity distribution from predominantly lateral to vertical. Consistent with the discussion above, the salinity varies mainly vertically only for sufficiently strong lateral tidal mixing fluxes.

#### b. Cross-sectionally averaged salt fluxes and $S_x$

As expected from the solutions of u and s, the salt flux us due to the exchange flow is characterized by lateral variability for weaker lateral transport and by vertical variability for stronger lateral transports (Fig. 3). The mechanism by which the salt balance is maintained by the exchange flow differs for weak and strong lateral mixing. For smaller lateral mixing, saltier water in the channel center is mainly transported up the estuary, while for greater lateral mixing, fresher water is mainly transported toward the ocean closer to the surface.

These solutions of us are next used to compute the cross-sectionally averaged salt flux  $(\overline{h})^{-1}\overline{\langle us \rangle}$  to then determine  $\Gamma$  for a range of  $\gamma$ , which is directly related to the dimensional salt flux through (28) (Fig. 4). The dependency of  $\Gamma$  on  $\gamma$  agrees well with the theoretical expectations for weak and

strong lateral transports; see (22) and (26), respectively. Because |us| decreases with lateral mixing, so does  $\Gamma$ .

Equipped with  $\Gamma(\gamma)$  for the particular channel geometry (recall here a bilinear depth profile), we next explore how lateral mixing affects the cross-sectionally along-channel salinity distribution S(x) or its gradient  $S_x(x)$  through (30). As an example, we take  $\gamma = 0.1$  ( $\Gamma \approx 0.014$ ) and  $\gamma = 1$  ( $\Gamma \approx 0.007$ ) and consider a range of river discharge values from  $Q = (1\,101\,001\,000)\,\mathrm{m}^3\,\mathrm{s}^{-1}$ , which is related to U through  $Q = UBh_0/2$  (Fig. 5). Note that the  $\gamma$  values are consistent with observations, as discussed below. These results illustrate that increasing lateral mixing through  $K_{MY}$  by a factor of 10 (i.e.,  $\gamma_M$  increases by a factor of 10) decreases the salinity intrusion length by half. This decrease is comparable to the effect of decreasing the river discharge by a factor of 10.

Because  $L_E$  scales inversely with vertical mixing as  $(K_{MZ}^2K_{SZ})^{-1/3}$ , it has been suggested that reduced vertical mixing by increased river discharge has a compensating effect on the salinity intrusion length (Monismith et al. 2002), consistent with observations of a relatively weak salinity response to river discharge (Garvine et al. 1992). In our study, this compensating effect is weakened (assuming lateral mixing is relatively unaffected by discharge) as for small  $\gamma = \gamma_S$ , the salinity intrusion length scales as  $K_{SZ}^{-2/3}K_{SY}^{-1/3}$ , whereas for large  $\gamma = \gamma_S$ , the

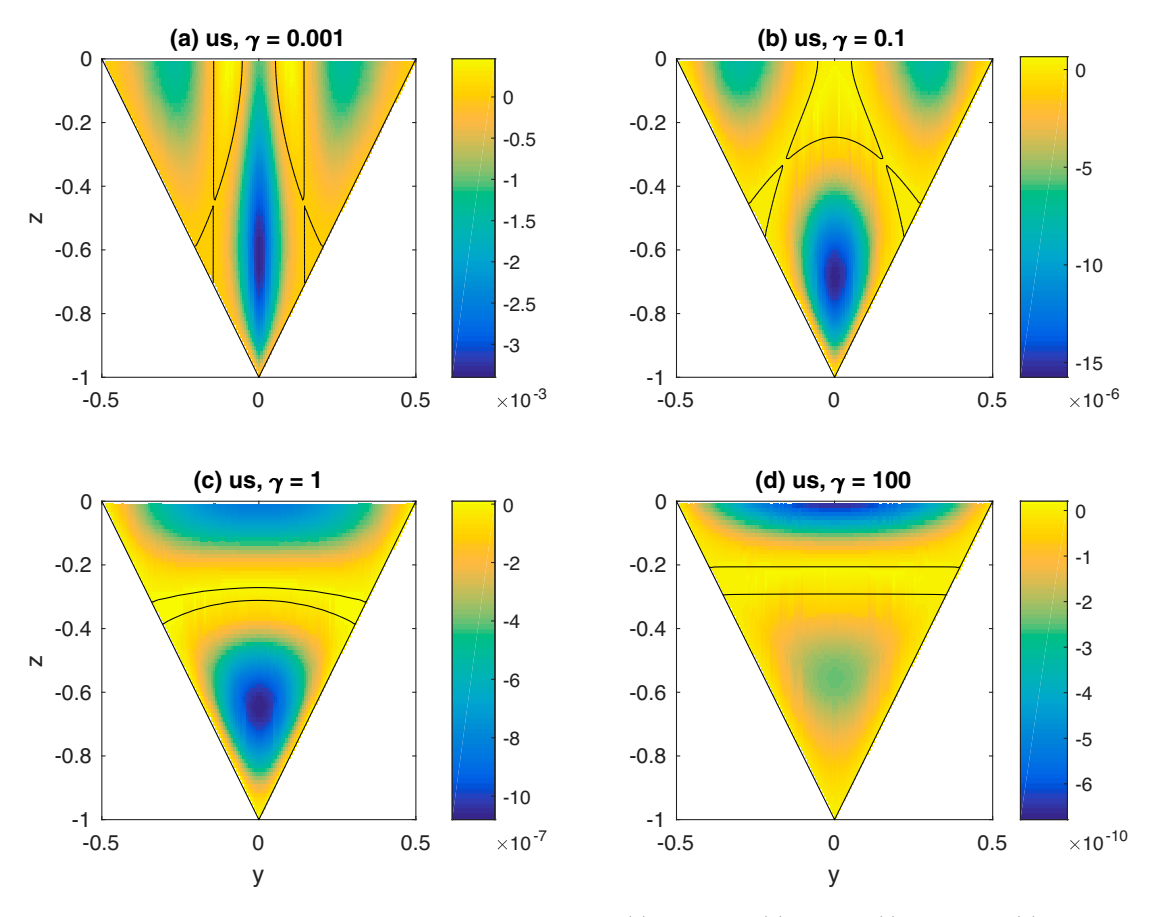


FIG. 3. Nondimensional numeric solutions of the salt flux us for (a)  $\gamma = 0.001$ , (b)  $\gamma = 0.1$ , (c)  $\gamma = 1$ , and (d)  $\gamma = 100$ . Black lines show us = 0.

salinity intrusion length scales as  $K_{SZ}^{-1/3}K_{SY}^{-2/3}$ . Thus, lateral transport exerts a critical control on the along-estuary salinity distribution.

## 5. Estimates of Fischer number $\gamma$

In the following discussion, we attempt to estimate observationally  $\gamma$  and assume again  $K_{MY} = K_{SY}$  and  $K_{MZ} = K_{SZ}$  so that  $\gamma = \gamma_M = \gamma_S$ . This is generally challenging because 1) observations of lateral dispersion in estuaries are limited and 2) tidally averaged lateral dispersion includes multiple tidally resolved and averaged processes (see introduction). One of the few studies that we are aware of that reports direct estimates of both vertical and lateral mixing and related time scales is that of Geyer et al. (2008). In particular, the observed tidally averaged lateral dispersion estimates were consistent with shear dispersion due to lateral currents sheared vertically. Based on a series of dye releases, they report estimates of lateral diffusivities in the range of 0.4–1.7 m<sup>2</sup> s<sup>-1</sup> and found that this lateral mixing rate was consistent with dispersion due to vertical shear of lateral velocities. These estimates of lateral mixing correspond to lateral mixing times of 0.5-1.5 days. Interestingly, little evidence of spring/neap variability in lateral mixing was observed although mixing estimates may be limited by geometric constraints of the channel. In contrast, vertical mixing

was strongly influenced by the spring/neap cycle and increased nearly an order of magnitude with estimates increasing from  $4\times 10^{-5}$  m² s<sup>-1</sup> during neap to  $2\times 10^{-4}$  m² s<sup>-1</sup> during spring tides, which represents estimates in the pycnocline and is, thus, more representative of a minimum in diffusivity in the water column. These estimates correspond to vertical mixing time scales of 6 days during neap and 16 h during spring tides. Note that a more general approach needs to take into account the tidal time scale relative to the mixing time scale (Geyer and MacCready 2014), which is beyond the scope of this study. Therefore, these observations indicate that  $\gamma$  varies between 4 and 12 during neap tides and 0.4–1 during spring tides. According to our results, these estimates based on the Geyer et al. (2008) study result in an increased lateral variability of salt and momentum during spring tides, which is consistent with observations.

An alternative estimate for  $\gamma$  can be derived for the homogeneous open channel flow following Fischer (1976), who approximated  $K_{SY} \sim 1.0 u_* \overline{h}$  for some river systems, where  $u_*$  is an averaged bottom friction velocity due to tidal currents. In particular, a dye release in Delaware Bay reported by Fischer (1976) yielded a numeric value of  $K_{SY}$  consistent with that from Geyer et al. (2008). Taking the Fischer (1976) estimate  $K_{SZ} \sim 0.07 u_* \overline{h}$  for homogeneous open channel flows yields  $\gamma_s \sim 14\delta^2$ , which is likely an underestimate because  $K_{SZ}$  can be substantially reduced due to vertical stratification. Furthermore,

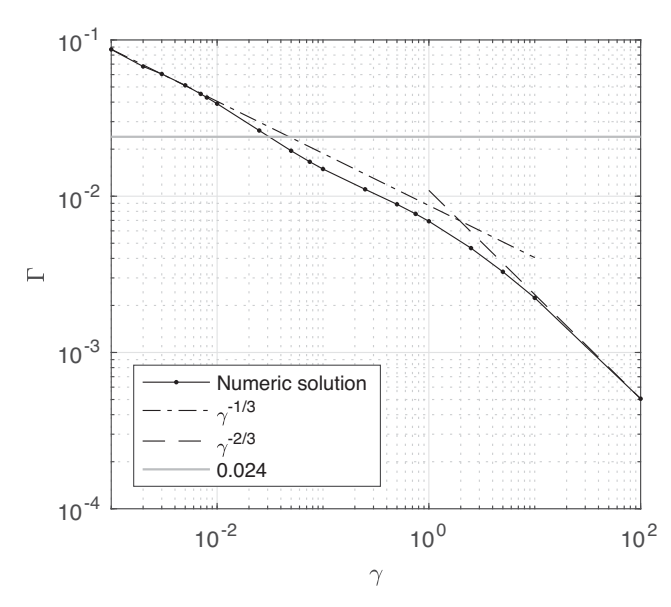


FIG. 4. Solutions for  $\Gamma(\gamma)$ : numeric (solid line; dot for each simulation run), theory for  $\gamma \ll 1$  ( $\Gamma \propto \gamma^{-1/3}$ ; dash-dotted line), theory for  $\gamma \gg 1$  ( $\Gamma \propto \gamma^{-2/3}$ ; dashed line), and the constant value for classic estuarine circulation theories (solid gray; MacCready and Geyer 2010).

Fischer (1976) discussed the potential role of shoreline irregularities and secondary circulations so that  $K_{SY}$  may scale with B, rather than depth. Banas et al. (2004) suggest that  $K_{SY}$  scales with tidal excursion for wide channels. Therefore, both vertical and lateral dispersion coefficients may scale with the tidal amplitude to constrain the variability of  $\gamma$ . In this case, one may expect for constant density flows that  $K_Y \sim u_*B$  and  $K_Z \sim u_*h_0$  and  $\gamma \sim \delta$ .

In wider estuaries, such as Delaware Bay, one might expect  $\gamma$  to be smaller as the lateral mixing time could be large. Yet, both Geyer et al. (2020) and Aristizábal and Chant (2013) suggest that the effective width of the system is not much wider than the main thalweg where most of the upstream salt flux occurs. Thus, we suspect that  $\gamma$  may also be related to the relevant effective width. In addition, lateral salinity gradients will increase with vertical mixing and potentially produce stronger lateral flows and lateral mixing, thus limiting the variability of  $\gamma$ . Similarly, weak vertical mixing yields stronger stratification which reduces lateral flows and, thus, limits lateral mixing which again limits the variability of  $\gamma$ . The general dependence of the horizontal and vertical exchange processes suggests that the range of  $\gamma$  is constrained. Nevertheless, because vertical mixing varies over multiple orders of magnitude, one may anticipate that  $\gamma$  also varies over several magnitudes. Our study suggests that it is critical to better understand the complex physics of lateral transport in order to better characterize the estuarine exchange flow.

### 6. Conclusions

This study extends the classic model of the gravitationally driven tidally averaged estuarine circulation, also referred to as the residual circulation or exchange flow, by including lateral (across the estuarine width) transport processes focusing on lateral tidal mixing. We demonstrate that the lateral transport of

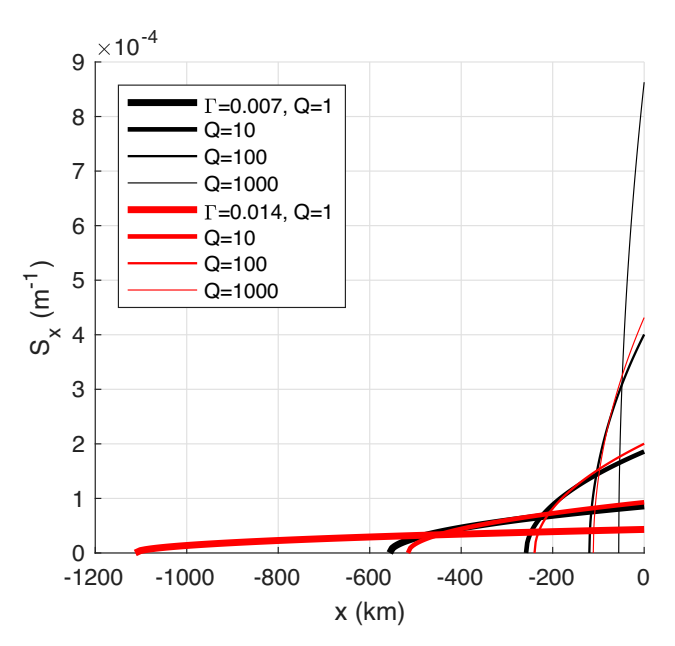


FIG. 5. Analytic solutions  $S_x(x)$  for  $\Gamma = 0.007$  (black) and  $\Gamma = 0.014$  (red) and river discharges  $Q = [1, 10, 100, 1000] \text{ m}^3 \text{ s}^{-1}$ , which is related to U through  $Q = UBh_0/2$ .

salt is essential for closing the steady-state salt budget and, thus, for maintaining the residual circulation. In this study, we focus on tidally averaged lateral tidal mixing fluxes that mix properties from high to low concentrations.

To understand the influence of such lateral transport on the residual circulation, we devise an idealized steady-state model that conserves momentum and salt mass. For tidal-mixing-fluxdominated regimes, we show that solutions for the along-estuary velocity and salinity deviations from its cross-sectional average can be nondimensionalized to depend on a key nondimensional parameter that describes the relative importance of horizontal to vertical tidal mixing, which is referred to as the Fischer number  $\gamma$ . Analytic considerations demonstrate that for relatively weak lateral tidal mixing (small  $\gamma$ ), lateral tidal mixing can be neglected in the momentum equation but is critical for the salt budget and along-estuary salt fluxes due to the exchange flow scale inversely with  $\gamma$ . For the other extreme of the relatively strong lateral tidal mixing (large  $\gamma$ ), lateral tidal mixing is dominant over vertical mixing in the momentum equation and along-estuary salt fluxes scale with the inverse squared  $\gamma$ . It is shown that these results directly impact the cross-sectionally averaged salinity distribution along the channel and that the estuarine salinity intrusion length scales also inversely with  $\gamma$ .

Analytic predictions agree well with two-dimensional numeric solutions for an idealized bilinear depth profile. Overall, these solutions are characterized by substantial lateral transport due to tidal mixing and variability that strongly depends on  $\gamma$ . For greater lateral tidal mixing (greater  $\gamma$ ), salinity predominantly varies with depth. On the other hand, for relatively weak lateral tidal mixing (smaller  $\gamma$ ), salinity mainly depends on lateral location, which sets up strong lateral density gradients. Because lateral transport affects the estuarine residual circulation, it also exerts a critical control on the along-estuary salinity distribution. Lateral

density gradients furthermore result in sustained lateral flows with surface convergence regions in the channel center in which the buoyant material is expected to aggregate. If these lateral flows are sufficiently strong, advection may become dynamically important, which will be investigated in a follow-up investigation. Overall, this study demonstrates that lateral transport controls the estuarine residual circulation and needs to be considered in more comprehensive concept models.

Acknowledgments This work was supported by the U.S. National Science Foundation (Awards OCE-2148370 and OCE-2148375) and NOAA MDP (Awards NA21NOS9990110, NA19NOS9990083, and NA19NOS9990084). We thank three anonymous reviewers for their detailed and constructive comments that have improved the manuscript.

Data availability statement This research is based on theoretical work without numerical or observational datasets that can be shared beyond what is presented here.

#### REFERENCES

- Aristizábal, M., and R. Chant, 2013: A numerical study of salt fluxes in Delaware Bay estuary. *J. Phys. Oceanogr.*, **43**, 1572–1588, https://doi.org/10.1175/JPO-D-12-0124.1.
- Banas, N. S., B. M. Hickey, and P. MacCready, and J. A. Newton, 2004: Dynamics of Willapa Bay, Washington: A highly unsteady, partially mixed estuary. *J. Phys. Oceanogr.*, **34**, 2413–2427, https://doi.org/10.1175/JPO2637.1.
- Burchard, H., R. D. Hetland, E. Schulz, and H. M. Schuttelaars, 2011: Drivers of residual estuarine circulation in tidally energetic estuaries: Straight and irrotational channels with parabolic cross section. *J. Phys. Oceanogr.*, 41, 548–570, https:// doi.org/10.1175/2010JPO4453.1.
- Chatwin, P. C., 1976: Some remarks on the maintenance of the salinity distribution in estuaries. *Estuarine Coastal Mar. Sci.*, 4, 555–566, https://doi.org/10.1016/0302-3524(76)90030-X.
- Fischer, H. B., 1972: Mass transport mechanisms in partially stratified estuaries. *J. Fluid Mech.*, 53, 671–687, https://doi.org/10.1017/S0022112072000412.
- ——, 1976: Mixing and dispersion in estuaries. Annu. Rev. Fluid Mech., 8, 107–133, https://doi.org/10.1146/annurev.fl.08.010176. 000543.
- Garvine, R. W., R. K. McCarthy, and K.-C. Wong, 1992: The axial salinity distribution in the Delaware estuary and its weak response to river discharge. *Estuarine Coastal Shelf Sci.*, **35**, 157–165, https://doi.org/10.1016/S0272-7714(05)80110-6.
- Geyer, W. R., and P. MacCready, 2014: The estuarine circulation. Annu. Rev. Fluid Mech., 46, 175–197, https://doi.org/10.1146/annurev-fluid-010313-141302.
- —, R. Chant, and R. Houghton, 2008: Tidal and spring-neap variations in horizontal dispersion in a partially mixed estuary. J. Geophys. Res., 113, C07023, https://doi.org/10. 1029/2007JC004644.
- —, D. K. Ralston, and J.-L. Chen, 2020: Mechanisms of exchange flow in an estuary with a narrow, deep channel and wide, shallow shoals. *J. Geophys. Res. Oceans*, **125**, e2020JC016092, https://doi.org/10.1029/2020JC016092.
- Hansen, D. V., and M. Rattray Jr., 1965: Gravitational circulation in straits and estuaries. *J. Mar. Res.*, 23, 104–122.

- Huzzey, L. M., and J. M. Brubaker, 1988: The formation of longitudinal fronts in a coastal plain estuary. *J. Geophys. Res.*, **93**, 1329–1334, https://doi.org/10.1029/JC093iC02p01329.
- Jay, D. A., and J. D. Musiak, 1994: Particle trapping in estuarine tidal flows. J. Geophys. Res., 99, 20445–20461, https://doi.org/ 10.1029/94JC00971.
- Lacy, J. R., M. T. Stacey, J. R. Burau, and S. G. Monismith, 2003: Interaction of lateral baroclinic forcing and turbulence in an estuary. J. Geophys. Res., 108, 3089, https://doi.org/10.1029/ 2002JC001392.
- Lerczak, J. A., and W. R. Geyer, 2004: Modeling the lateral circulation in straight, stratified estuaries. *J. Phys. Oceanogr.*, **34**, 1410–1428, https://doi.org/10.1175/1520-0485(2004)034<1410: MTLCIS>2.0.CO;2.
- Li, M., P. Cheng, R. Chant, A. Valle-Levinson, and K. Arnott, 2014: Analysis of vortex dynamics of lateral circulation in a straight tidal estuary. *J. Phys. Oceanogr.*, 44, 2779–2795, https://doi.org/10.1175/JPO-D-13-0212.1.
- MacCready, P., and W. R. Geyer, 2010: Advances in estuarine physics. *Annu. Rev. Mar. Sci.*, 2, 35–58, https://doi.org/10. 1146/annurev-marine-120308-081015.
- Majda, A. J., and P. R. Kramer, 1999: Simplified models for turbulent diffusion: Theory, numerical modelling, and physical phenomena. *Phys. Rep.*, 314, 237–574, https://doi.org/10.1016/S0370-1573(98)00083-0.
- Monismith, S. G., W. Kimmerer, J. R. Burau, and M. T. Stacey, 2002: Structure and flow-induced variability of the subtidal salinity field in northern San Francisco Bay. *J. Phys. Oceanogr.*, 32, 3003–3019, https://doi.org/10.1175/1520-0485(2002)032<3003: SAFIVO>2.0.CO;2.
- Nunes, R. A., and J. H. Simpson, 1985: Axial convergence in a well-mixed estuary. *Estuarine Coastal Shelf Sci.*, 20, 637–649, https://doi.org/10.1016/0272-7714(85)90112-X.
- Ralston, D. K., W. R. Geyer, and J. A. Lerczak, 2008: Subtidal salinity and velocity in the Hudson River estuary: Observations and modeling. *J. Phys. Oceanogr.*, 38, 753–770, https://doi.org/10.1175/2007JPO3808.1.
- Scully, M. E., W. R. Geyer, and J. A. Lerczak, 2009: The influence of lateral advection on the residual estuarine circulation: A numerical modeling study of the Hudson River estuary. *J. Phys. Oceanogr.*, 39, 107–124, https://doi.org/10.1175/2008JPO3952.1.
- Smith, R., 1976: Longitudinal dispersion of a buoyant contaminant in a shallow channel. *J. Fluid Mech.*, **78**, 677–688, https://doi.org/10.1017/S0022112076002681.
- Taylor, G. I., 1953: Dispersion of soluble matter in solvent flowing slowly through a tube. *Proc. Roy. Soc. London*, 219A, 186– 203, https://doi.org/10.1098/rspa.1953.0139.
- Thoman, T. X., T. Kukulka, and K. Gamble, 2021: Dispersion of buoyant and sinking particles in a simulated wind- and wave-driven turbulent coastal ocean. *J. Geophys. Res. Oceans*, **126**, e2020JC016868, https://doi.org/10.1029/2020JC016868.
- Valle-Levinson, A., 2008: Density-driven exchange flow in terms of the Kelvin and Ekman numbers. J. Geophys. Res., 113, C04001, https://doi.org/10.1029/2007JC004144.
- —, and L. P. Atkinson, 1999: Patial gradients in the flow over an estuarine channel. *Estuaries*, **22**, 179–193, https://doi.org/10.2307/1352975.
- —, K.-C. Wong, and K. M. M. Lwiza, 2000: Fortnightly variability in the transverse dynamics of a coastal plain estuary. *J. Geophys. Res.*, 105, 3413–3424, https://doi.org/10.1029/1999JC900307.
- Wong, K.-C., 1994: On the nature of transverse variability in a coastal plain estuary. *J. Geophys. Res.*, 99, 14209–14222, https:// doi.org/10.1029/94JC00861.